Fabrication and Performance of Silicon-Embedded Permanent-Magnet Microgenerators

Florian Herrault, Bernard C. Yen, *Member, IEEE*, Chang-Hyeon Ji, *Member, IEEE*, Zoltan S. Spakovszky, Jeffrey H. Lang, *Fellow, IEEE*, and Mark G. Allen, *Senior Member, IEEE*

***Abstract*—This paper focuses on the design, fabrication, and characterization of silicon-packaged permanent-magnet (PM) microgenerators. The use of silicon packaging favors fine control on shape and dimensions in batch fabrication and provides a path toward high rotational speeds (∼1 Mr/min), a requirement for ultimate compactness of microgenerators. The successful silicon packaging of these microgenerators consisted of three essential elements: 1) a winding scheme allowing both nonplanar fabrication and through-wafer interconnects; 2) laminations built into the silicon for enhanced electrical performance; and 3) a balancing scheme for the heavy PM rotor to ensure its maximum performance. The devices were fabricated using bonded silicon wafers, integrated magnetics, and an electroplated metal. The mechanical strength of the 12-mm-diameter silicon-packaged PM rotors was evaluated at high rotational speeds using an external spindle drive. Speeds up to 200 000 r/min were achieved prior to a mechanical rotor failure. The generators were electrically characterized, and an output power in excess of 1 W across a resistive load of 0.32 Ω was measured at a maximum speed. A 225% power increase was also experimentally determined due to the addition of a laminated stator back iron. [2009-0151]**

***Index Terms*—AC generators, interconnects, laminations, microgenerator, permanent magnets (PMs), silicon packaging.**

I. Introduction

RECENT ADVANCES in the technology and performance of electronic devices have driven the development of new systems of power generation. Several research groups have dedicated their attention toward rotational permanent-magnet (PM) microgenerators as a component of chemical-to-electrical converters such as fuel-powered microengines [1], [2]. In principle, the magnetic flux density that is available from a PM is not dependent on its size [3]. Therefore, microgenerators using PMs as a constant source of magnetic flux are attractive, and the advances in microelectromechanical systems (MEMS) fabrication technology enable the incorporation of new magnetic materials (soft and hard magnetics) as well as multilayer microcoils. In operation, a spinning rotor with alternating magnetic poles generates a time-varying magnetic field, which induces ac voltages in the stator windings that are positioned underneath the rotor (Faraday's law). When the winding terminals are connected to an external load, the device generates electrical power. PM microgenerators, with rotor dimensions varying from 2 to 12 mm, have been reported with output power ranging from microwatts to tens of watts [4]–[9]. The devices consist of rotors with either discrete PM pieces [8], [9] or magnetically patterned PM rings [4]–[7], [10] together with microfabricated copper coils. An external turbine provides mechanical input power to the rotor. The design and performance comparisons are detailed in [11] and [12]. As an ongoing effort toward integration and packaging, compact power generators combining an electrical microgenerator and a small-scale air-driven turbine have been presented [13], [14]. These devices used ball bearings to support the rotor. Because the turbines and associated fluidic packages were formed from laser-machined polymers, these devices were limited to low-temperature applications.

Silicon packaging offers the possibility of fine control on the shape and dimensions of batch-fabricated devices. Tight tolerances are required to operate microgenerators at high rotational speeds, which would result in high power densities, a major goal for ultimate compactness. It has been demonstrated that the fabrication of small-scale gas bearings for high-rotational-speed operation is compatible with silicon technology [15]–[18]. Gas-bearing-supported microturbines have demonstrated an ultrahigh-speed operation (beyond 1 Mr/min). Aside from higher rotor speeds, other advantages over simpler designs using ball bearings are lifetime and stability of operation. Furthermore, silicon packaging facilitates the coupling of microgenerators with high-temperature high-power-density microengines that utilize the combustion of hydrocarbon fuels as an energy source. In [19], we have confirmed that MEMS-scale PM generators are suitable for high-temperature applications with careful selection of materials. The PM rotor used SmCo magnets, and the 10-mm-diameter device demonstrated a watt-level output power at relatively high temperatures (100 °C–300 °C).

The major difficulty in achieving silicon packaging is caused by the divergence in fabrication approaches, as well as inconsistencies in requirements between a silicon structure and the magnetic and winding components. The integration challenges consist of the following: 1) the fabrication of microfabricated

Manuscript received June 11, 2009; revised October 13, 2009. First published December 8, 2009; current version published February 3, 2010. This work was supported in part by the Army Research Laboratory (DAAD19-01-2-0010) under the Collaborative Technology Alliance in Power and Energy program. Subject Editor R. R. A. Syms.

F. Herrault, C.-H. Ji, and M. G. Allen are with the School of Electrical and Computer Engineering, Georgia Institute of Technology, Atlanta, GA 30332 USA (e-mail: fh59@mail.gatech.edu; cji6@mail.gatech.edu; mark.allen@ece.gatech.edu).

B. C. Yen was with the Department of Electrical Engineering and Computer Science, Massachusetts Institute of Technology, Cambridge, MA 02139 USA. He is now with BioScale, Inc., Cambridge, MA 02139 USA (e-mail: bernardy@usa.net).

Z. S. Spakovszky and J. H. Lang are with the Massachusetts Institute of Technology, Cambridge, MA 02139 USA (e-mail: zolti@mit.edu; lang@mit.edu).

Color versions of one or more of the figures in this paper are available online at http://ieeexplore.ieee.org.

Digital Object Identifier 10.1109/JMEMS.2009.2036583

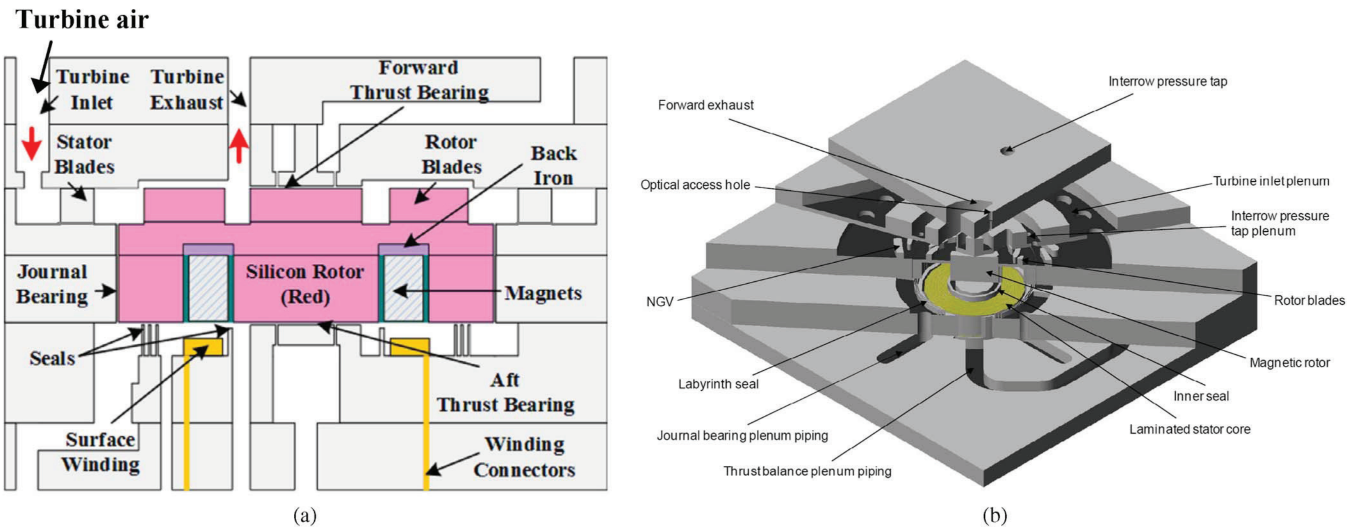

Fig. 1. (a) Cross-sectional schematics of the silicon-packaged gas-bearing-supported PM generator with an integrated microturbine. The device was constructed on a seven-wafer silicon stack. (b) Cutaway 3-D rendering of the device. Note that the rotor magnetics and the windings are not depicted for ease of viewing.

windings having through-wafer interconnects inside a 3-D microstructure; 2) the integration of a laminated stator back iron for enhanced electrical performance; and 3) the conception of a balanced rotor for high-speed operation and maximum rotor performance.

In order to address the winding and interconnect challenges, a drop-in approach is proposed and consists of decoupling the fabrication of the copper windings from the silicon stator structure. The windings are fabricated on a different substrate and subsequently released. This is followed by manual insertion of the coils inside a dedicated recess in the silicon structure. The electrical interconnects were constructed with the coils and then manually folded and threaded via through-wafer silicon openings for backside electrical connections. The integration of the vertically laminated stator back iron was implemented by etching trenches in the silicon stator and subsequently electroplating Permalloy. To minimize the imbalance of the rotor, a configuration that used discrete pieces of magnetic materials was utilized, together with high-precision laser micromachining of the magnetics and with a specific assembly protocol.

We have recently presented the performance of a preliminary silicon-packaged microgenerator coupled with a gas-bearing-supported microturbine, as shown in Fig. 1 [20]. The device consisted of a free-standing silicon magnetic rotor and an electrical stator. The rotor and the integrated microturbine were supported by a gas journal bearing in the radial direction and gas thrust bearings in the axial direction. As pointed out in Fig. 1(a), turbine air was added to accelerate the rotor. A high-speed operation was achieved when the rotor was spinning in supercritical mode (i.e., above the journal bearing natural frequency) [21]. This device was fabricated from seven silicon wafers, with the first five fusion-bonded to form the upper die and the remaining two fusion-bonded to form the bottom die. It experimentally demonstrated an output power of 19 mW across a resistive load at a rotational speed of 40 000 r/min [20], [21]. The maximum achieved power was limited by gas bearing challenges due to the clamped nature of the package, as well as the lack of magnetic stator laminations.

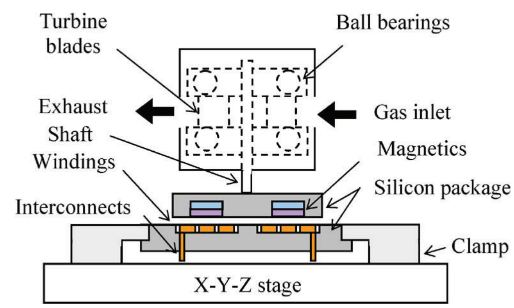

Fig. 2. Rendering of the experimental setup showing the silicon-packaged PM microgenerator and the external spindle drive.

In this paper, we detail the fabrication approaches developed to address the challenges associated with silicon packaging of PM microgenerators. The devices, which do not include a microturbine, consist of a microfabricated stator copper coil with integrated magnetic laminations in a silicon frame as well as a silicon-based rotor with inserted magnetics (i.e., ferromagnetic back iron and PMs). Using an external spindle to drive the rotor, the maximum performance of silicon-packaged microgenerators was investigated. This experimental setup is shown in Fig. 2. This characterization includes rotor mechanical failure, stator electrical measurements, open-circuit voltages, and electrical power measured across resistive loads. The objectives of this paper are to test the structural integrity of the 12-mm-diameter silicon rotor with inserted magnetics and to demonstrate the power generation and viability of the fabricated stators packaged with silicon. The measured performance also provides conditions for achieving a watt-level output power.

Following this introduction, the key elements required for successful silicon packaging of PM microgenerators are detailed. First, the integration of microfabricated windings and through-wafer interconnects is presented, followed by the fabrication process and the experimental results. Second, the design and fabrication of magnetic stator laminations within a silicon structure are described. Third, the rotor design and balancing scheme is explained, including the microfabrication

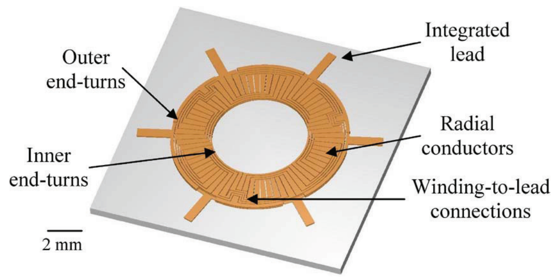

Fig. 3. Rendering of gas-bearing-compatible stator windings.

of the magnetics as well as the assembly protocol. Finally, the experimental results achieved using an external spindle drive are presented and discussed.

II. Drop-In Winding and Interconnect Technology

The integration of multilayer electrodeposited metal structures into nonplanar topographies is challenging primarily due to the difficulties associated with forming reasonably thick precisely patterned molds on these types of structures. Although some success was achieved using ultrathick spin-coated photoresists [22], spray coating [23], [24], or electrodeposited resists [25] to pattern molds at the bottom of high-aspect-ratio cavities, these approaches suffer from resolution and aspect-ratio limitations, due to the diffraction effect of photolithography. Alternative approaches were investigated such as one involving the chemical vapor deposition of a polymer inside recesses, followed by laser microablation to form electroplating molds [26]. Although this technology demonstrated satisfactory resolution and process capabilities, the serial nature of laser ablation was a major constraint. Consequently, an alternative fabrication approach was proposed to integrate multilayer metal microstructures into complex 3-D devices. This technology relies on the separate fabrication of the silicon structure and the free-standing metal windings, followed by manual insertion of the coils inside the silicon device.

A. Winding Design Overview

The microfabricated windings are three-phase, eight-pole, and three-turn coils. The three phases exhibit a 30° mechanical angle between each other. The arrangement of the surface-wound conductors greatly benefited from microfabrication technologies by defining an intricate pattern, which resulted in the increase of the filling factor (ratio between the volume of copper conductors and the overall utilized volume). Preliminary versions of the stator coils were designed and fabricated to demonstrate the feasibility of high-power-density devices [4], [5], [7]. Specific details of the winding arrangement can be found in [7]. However, these proof-of-concept devices were not designed for integration with a complex 3-D silicon structure because they were fabricated onto a thick ferromagnetic substrate without size requirements and the constraints of the backside interconnection.

As a result, several design changes were made, as shown in Fig. 3. In this version, the inner diameter was 5.4 mm, and the outer diameter was 9.7 mm. The coils were 200 μm thick,

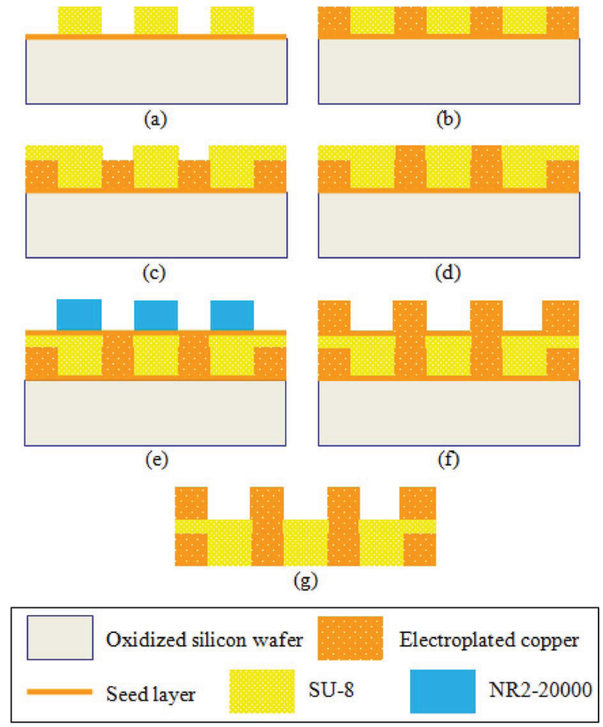

Fig. 4. Drop-in winding fabrication process flow: [(a) and (b)] First copper layer electroplating, [(c) and (d)] via layer fabrication, [(e) and (f)] second copper layer, and (g) device release. The bottom and top copper layers are between 80 and 100 μm thick, with a 40-μm lateral gap between conductors. The insulation layer between the two copper layers is approximately 40 μm thick.

which consisted of a coil volume reduction of 2.3 times over [7], reducing the net output power delivered by the device. These dimension changes were dictated by the design of the gas-bearing-supported device (Fig. 1) [21]. A through-wafer connection scheme was developed by fabricating integrated copper leads, followed by a manual 90° folding and insertion through via holes etched in the silicon stator.

B. Fabrication Process and Results

The drop-in windings were created using a three-layer copper electroplating process combined with primarily SU-8 epoxy micromolding. First, a 0.5-μm-thick plasma-enhanced chemical vapor deposition SiO_2 layer was deposited onto a rigid silicon substrate (100-mm diameter). A Ti/Cu/Ti seed layer was sputter deposited, and SU-8 2025 was used to pattern the first-layer electroplating mold [Fig. 4(a)]. Copper was then electrodeposited at a current density of approximately 10 mA/cm^2. The electrodeposition process was stopped when the copper was of the same level with the top of the mold, in order to obtain as flat a surface as possible [Fig. 4(b)]. A second layer of SU-8 2025, labeled "via layer," was spin coated and patterned to open vias between top and bottom copper layers [Fig. 4(c)]. This layer also acted as an insulation layer. The vias were electroplated [Fig. 4(d)]. A second Ti/Cu/Ti seed layer was sputter deposited, and the third electroplating mold was patterned using a negative photoresist (NR2-20000, Futurrex, Inc.) [Fig. 4(e)]. Copper was again electrodeposited to form the top layer [Fig. 4(f)]. The photoresist was stripped using a combination

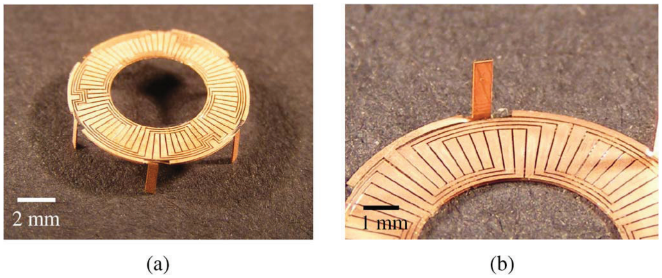

Fig. 5. Photographs of the drop-in windings with integrated folded electrical connections: (a) Full view and (b) close-up view. The six copper leads were folded at a 90° angle. The copper filling factor was at approximately 90%.

of acetone and O_2 plasma reactive ion etching (RIE). The SiO_2 layer, which was deposited at the very beginning of the process, was then etched away in concentrated hydrofluoric acid to release the three-layer copper coils from the rigid silicon substrate. The two seed layers were removed using a solution of NH_4OH saturated with $CuSO_4$ to etch the copper and a bath of 1:50 HF : H_2O to etch titanium [Fig. 4(g)]. The SU-8 layer remaining in the center region and on the outer edges of the windings was laser ablated using an excimer laser after release. Finally, the six electrical leads were manually folded at a 90° angle using a dedicated jig to control the bending and orientation of the copper tabs. Fig. 5 shows the microfabricated windings with the folded electrical leads.

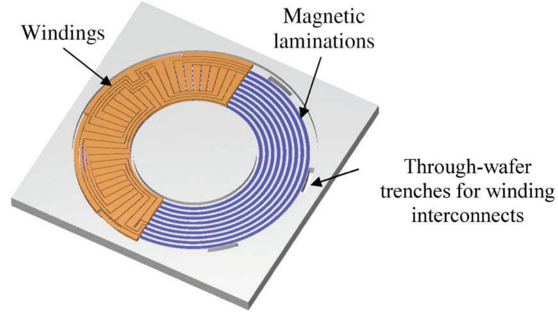

Fig. 6. Three-dimensional conceptual rendering of a magnetic stator. The dimensions of the laminations were increased for better clarity. The silicon spokes are not represented in this schematic.

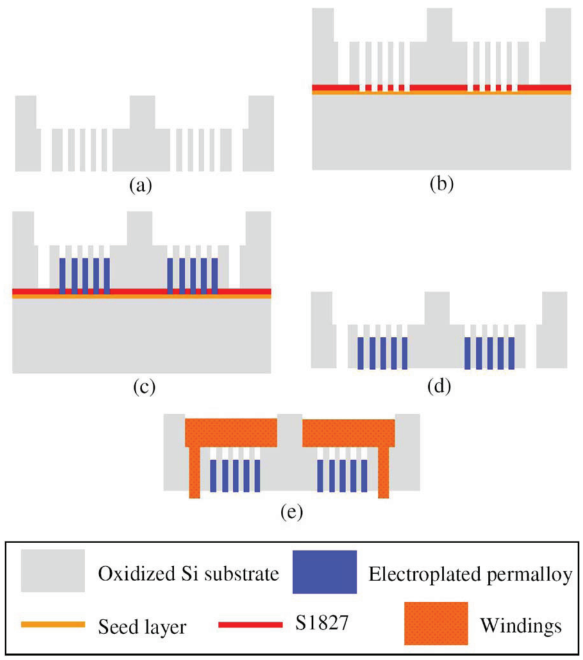

Fig. 7. Fabrication process flow of a vertically laminated Permalloy core in silicon and winding insertion. (a) Silicon etching of a front-side recess for winding insertion and backside trenches for electrical connections and magnetic laminated core. (b) Bonding of a seed wafer and patterning of the photoresist bonding layer for selective through-wafer plating. (c) Selective Permalloy plating. (d) Device release and seed layer removal. (e) Winding insertion.

III. Laminated Magnetic Stator Core

A. Lamination Design

The fabrication of a laminated magnetic stator core was also investigated to increase the device performance. The addition of a stator core greatly increases the magnetic flux in the machine, but it also generates more eddy current losses. Consequently, the magnetic material is laminated by alternating regions of magnetic and low-conductivity materials. The integration of vertically laminated magnetic cores in silicon has been previously reported [27]. This laminated version was fabricated by creating through-wafer circular trenches in the silicon wafer, and a ferromagnetic material (i.e., Permalloy $Ni_{80}Fe_{20}$) was subsequently electroplated in these trenches. Permalloy was selected as the electrodeposited ferromagnetic material for its high relative permeability (~800) and high saturation flux density (~1 T) [28]. The silicon lamination rings were held in place mechanically by five radial silicon spokes of a width of 50 μm. Fig. 6 shows a 3-D conceptual rendering of a laminated magnetic stator. For ease of viewing, the winding area was partially cleared, and the dimensions of the laminations were deliberately increased.

When designing laminated magnetic cores, the width of the magnetic laminations should be on the order of the skin depth of the magnetic material or less. The skin depth δ_m is given by

$$\delta_m = \frac{1}{\sqrt{\pi \cdot \mu_m \cdot \sigma_m \cdot f}} \tag{1}$$

where σ_m and μ_m are the conductivity and the permeability of the magnetic material, respectively, and f is the operating electrical frequency. The resistivity of the Permalloy was assumed to be 15 $\mu\Omega \cdot$ cm [29], and the operating frequency was about 20 kHz, which corresponded to a rotor speed of approximately 300 000 r/min for an eight-pole machine. As a result, 18 magnetic laminations having a width of 75 μm were designed. The silicon spacers were 50 μm in width to ensure their mechanical integrity. The height of the stator back iron was approximately 300 μm and was set by subtracting the depth of the winding recess from the thickness of the silicon wafers.

B. Fabrication of Laminated Stator Cores

First, a 250-μm-deep recess for winding insertion was fabricated by deep RIE (DRIE), using a Bosch process. This step was followed by a backside etching of through-wafer trenches, as shown in Fig. 7(a). As shown in Fig. 7(b), the oxidized silicon structure was bonded onto a seed wafer and

(a) (b)

Fig. 8. (a) Photograph of a silicon stator die with laminations before NiFe electroplating. (b) SEM micrograph of a vertically laminated electroplated Permalloy core.

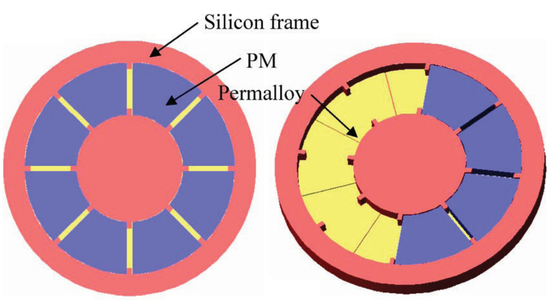

(a) (b)

Fig. 9. Schematics of a silicon-based rotor with integrated back iron and PMs. Note that the back iron pieces are staggered 22.5° with the PM pieces to form a continuous magnetic path.

used as the plating mold [Fig. 7(c)]. The magnetic material was electrodeposited from a temporarily bonded seed wafer using a bottom–up approach. It should be noted that the trenches fabricated for through-wafer electrical connections had to remain free of plating material, as shown in Fig. 6. As a result, the photoresist used as a bonding layer was selectively patterned prior to electrodeposition. The device was released by underetching the copper seed layer using an ammonium hydroxide solution saturated with copper sulfate. Although this was a relatively slow process, the copper etching solution is selective to Permalloy. Finally, the windings were inserted into the silicon stator, as shown in Fig. 7(e). A photograph of a silicon stator with through-wafer trenches and a SEM micrograph of the plated Permalloy are shown in Fig. 8.

IV. Balancing of Silicon Rotors With Inserted Magnetics

A. Rotor Design

The silicon-based magnetic rotor consisted of a silicon frame with inserted back iron and PM pieces, as shown in Fig. 9. The imbalance of a rotor is defined as the distance between the geometric center and the center of mass. To operate at its maximum performance, the rotor imbalance must be as low as possible. In the specific case of the gas-bearing-supported device, the rotor imbalance must be less than 5 μm [21]. Consequently, particular assembly techniques were developed to minimize the imbalance of the rotors as they were being fabricated. Although postassembly techniques such as mass removal by laser trimming or mass addition are commonly used to balance macroscale rotors, they appeared much more complicated approaches to implement for these microscale rotors. In addition, such techniques would require a characterization setup to identify the regions where materials should be removed or added. As a result, high-precision fabrication techniques must be used to build the silicon magnetic rotor. Silicon features, defined using a well-characterized DRIE tool, exhibit minimal imbalance. However, the laser machining of a thick PM material does not provide the same accuracy. In addition, the assembly of the magnetics (i.e., ferromagnetic back iron and PM pieces) inside the silicon frame was manual, which greatly increased the alignment errors. The silicon-packaged magnetic rotor was assembled using eight pie-shaped pieces for both the back iron and the PMs. Fig. 9 shows the current configuration. The "pie-piece" arrangement resulted in the least theoretical rotor imbalance, which was a critical parameter to achieve the rotor maximum performance. Detailed structural analysis and stress-related modeling of the different configurations can be found in [21]. The use of discrete pieces was more beneficial than a PM ring because they can be rearranged to compensate for machining tolerances. An imperfectly machined ring, on the other hand, introduces a large imbalance that cannot be easily corrected. The pieces were weighed and measured individually. To minimize the rotor imbalance, each of them was strategically located. In each slot, the outer edge of the magnetic pieces was pushed against the silicon frame. This was used to minimize the rotor imbalance by setting a similar outer radial position for each PM piece, thus reducing positioning errors and keeping micromachining inaccuracy closer to the inner radius. From a magnetic standpoint, the PM pieces were staggered 22.5° from the back iron pieces to establish a continuous magnetic circuit, as shown in Fig. 9(b).

B. Rotor Fabrication

The silicon frame consisted of two fusion-bonded silicon wafers of a combined thickness of 1.00 mm and a diameter of 12 mm. A 600-μm-deep annular cavity for the insertion of the magnetics was DRIE etched. The cavity had an inner radius of 2.5 mm and an outer radius of 5.0 mm. Silicon locators were defined in the cavity so that the integration of the magnetics would be facilitated. As mentioned previously, a drop-in approach was also applied for the magnetics.

In order to fabricate small-scale PMs with the angular shape of interest, a laser micromachining approach was utilized. We had demonstrated this technique for the fabrication of small-scale NdFeB and SmCo materials for ultraminiaturized PM generators [9]. Hence, 50-μm-thick NiFe back iron pieces and 500-μm-thick PM pieces were cut using a 1047-nm Nd:YLF laser. The back iron was laser machined at a cutting speed of 1 mm/s and an average power of 3.3 W [12]. The slabs of the PM materials were first demagnetized by heating them up to several hundred degrees Celsius. The materials were cut at a speed of 0.1 mm/s. Once the pieces were cleaned, they were fully remagnetized in the axial direction using a pulse-discharge magnetizer.

As shown in Fig. 10, this micromachining approach was successful for both SmCo and NdFeB materials at the scale of interest. Although the heat induced by the laser beam during the

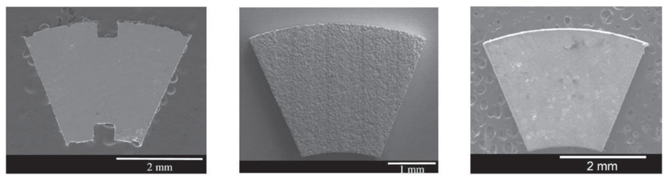

(a) (b) (c)

Fig. 10. SEM micrographs of the laser-machined microfabricated magnetics: (a) $Ni_{80}Fe_{20}$ back iron piece, (b) SmCo magnet, and (c) NdFeB magnet.

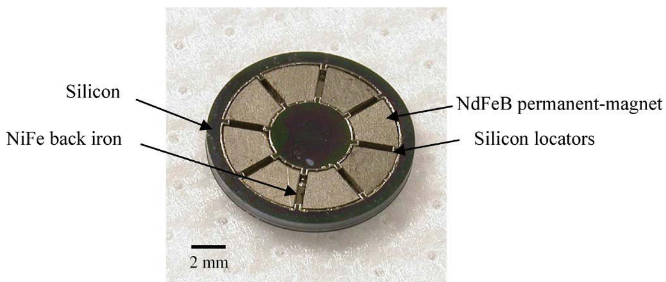

Fig. 11. Photograph of a silicon-packaged magnetic rotor.

machining affects the more temperature-sensitive NdFeB material, magnetic characterizations on millimeter-scale magnets [9], as well as calculations regarding the process scalability of this technique [12], have indicated that NdFeB magnets were more efficient than SmCo magnets at these dimensions. This was attributed to the low percentage of volume affected by the laser-induced degradation and by the higher remanence of NdFeB over SmCo at room temperature. As a result, NdFeB pie pieces were selected as the PM material for the air-driven silicon-packaged PM microgenerators. However, SmCo magnets would be used for integration with microengines, as they remain magnetized at high temperatures.

The rotor imbalance was primarily attributed to the PM pieces because they were ten times thicker than the back iron pieces. On average, the weight of the PM pieces was approximately 22.6 mg. Simulations were performed to estimate the maximum imbalance that allowed the rotor to cross the journal bearing natural frequency [21]. The results indicated that the maximum standard deviation between the weights of the PM pieces was limited to 0.1 mg. This corresponded to a 0.4% weight discrepancy between the PM pieces and a tolerance of 50 μm on the dimensions. Sets of eight PM pieces were laser machined and geometrically characterized. For a typical set of eight NdFeB magnets, the weight discrepancy was approximately 0.08 mg, which is less than the required value of 0.1 mg, and the dimension tolerances were on the order of 15–25 μm, which is well below 50 μm, validating the fabrication approach [12]. Magnets with similar weights were diametrically located, and the configuration that exhibited the least imbalance was selected. Similarly, the balancing scheme was applied to the back iron pie pieces. To improve the overall balance of the rotor, the pieces were also pushed against the outer edge of the silicon frame. Epoxy- or cyanoacrylate-based adhesives were used to bond the pieces inside the silicon rotor. One of the fabricated silicon magnetic rotors is shown in Fig. 11.

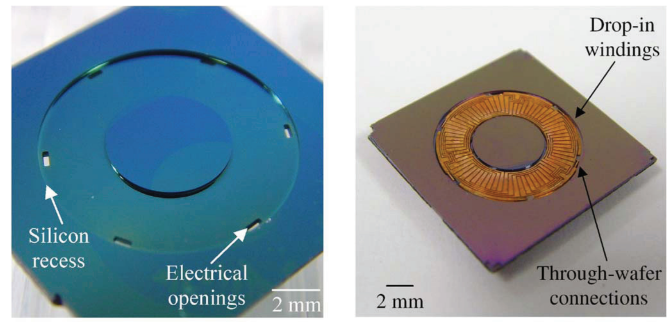

(a) (b)

Fig. 12. Photographs of a microfabricated silicon stator test structure (a) prior to the coil insertion and (b) with the integrated windings.

V. Silicon Stator Packaging

A. Silicon Stator Fabrication

Silicon structures were fabricated in order to ascertain the proper insertion of the drop-in windings. The radial dimensions of these were similar to the one set by the gas-bearing-supported design [16], [20]. First, a 250-μm-deep recess was DRIE etched from the front side of the wafer. The inner and outer radii measured 2.55 and 5.12 mm, respectively. After the removal of the etching mask and piranha cleaning, six through-wafer features for electrical connections were etched from the backside of the wafer. For the laminated stator configuration, the process presented previously was utilized. The interconnection features were 0.2 mm in width and 0.7 mm in length. In comparison, the copper leads that were inserted through these via holes were slightly smaller (0.15 and 0.5 mm) in order to facilitate the assembly process. An epoxy adhesive was subsequently added to the backside of the through-wafer connections to reduce potential gas leakage. For electrical insulation between the windings and the silicon stator, a 1-μm dry oxide layer was grown at 1100 °C.

Fig. 12(a) shows a photograph of a microfabricated silicon stator test structure. The windings with folded electrical connections (Fig. 5) were dropped into the recess, as shown in Fig. 12(b). Finally, six wires were soldered to the six copper leads protruding out of the backside of the silicon stator die.

B. Geometrical Characterization

To guarantee that there were no protrusions from the windings over the silicon surface, white light interferometry measurements were performed, as shown in Fig. 13. The results indicated that the windings were located below the surface throughout the entire area. These measurements demonstrate the viability of drop-in windings and the integration of multilayer electroplated microcoils into 3-D microstructures with complex geometries.

VI. Results

A. Experimental Setup

The setup, schematized in Fig. 2 and shown in Fig. 14, comprises x–y–z micropositioners and an external off-the-shelf turbine. Such a setup was used to measure the maximum

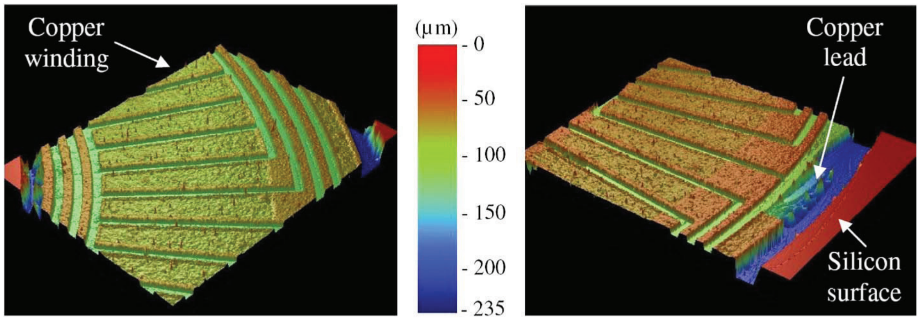

Fig. 13. Geometrical characterization of the integrated stator using white light interferometry. The windings are properly located below the silicon stator surface.

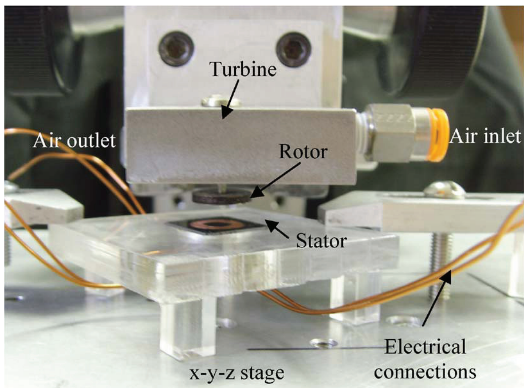

Fig. 14. Photograph of the microgenerator experimental setup. The air-driven turbine is encased in an aluminum housing. The air gap between the rotor and the stator was increased for visibility.

TABLE I
RESISTANCE AND INDUCTANCE MEASUREMENTS OF THE MICROFABRICATED WINDINGS AS A FUNCTION OF FREQUENCY USING AN IMPEDANCE ANALYZER

Frequency (kHz)	1	10	100
Rotor speed (krpm)	15	150	1,500
Resistance (mΩ)	319	321	320
Inductance (μH)	0.18	0.18	0.18
Inductive reactance (mΩ)	1.1	11.3	113.1

performance of the devices, independently of turbine or bearing limitations. The turbine was air driven and supported by two sets of high-speed ball bearings. A 1.6-mm-diameter stainless-steel shaft was used to connect the turbine to the backside of the silicon rotor housing, where a complementary recess had been fabricated. In order to guarantee proper alignment in both lateral and vertical directions, the shaft was first inserted and tightened into the turbine assembly. Using the micropositioners, the recess of the silicon rotor was carefully positioned below the shaft location. After that, the shaft was lowered inside the recess; a cyanoacrylate-based adhesive was applied to ensure good mechanical bond.

As shown in Fig. 14, the stator was placed into a test jig, and additional wires were soldered onto the stator electrical pads. The alignment between the rotor and the stator was set by monitoring the voltage waveforms generated by the device [9]. Using this test setup, mechanical failure of silicon rotors and electrical performance of the microgenerators were investigated.

B. Mechanical Failure of Silicon Rotors

Experimental mechanical failure tests of silicon magnetic rotors were performed so as to determine their maximum operating speed. A series of experiments was conducted, and it led to the following observations.

1) An empty silicon rotor without magnetics was spun up to 335 000 r/min without apparent degradation of its structural integrity. For this specific experiment, the rotational speed was recorded using a photodiode and a signal analyzer [29]. The rotational speed was limited by the turbine performance.
2) Rotors with glued magnetics systematically shattered in the 150–200-kr/min range.
3) The experimental setup was surrounded by a soft plastic housing to collect the broken pieces. Despite the full destruction of the silicon frame, the brittle magnets were still intact.
4) Cyanoacrylate-bonded rotors exhibited maximum speeds up to 15% higher than epoxy-bonded rotors, suggesting that the adhesion properties of the selected cyanoacrylate adhesive to silicon were better than that of the epoxy. The use of the cyanoacrylate adhesive was also more practical because of its fast drying time and its ability to be dissolved in acetone if the magnetics needed to be changed.

The authors attributed the mechanical failures of such silicon-based PM rotors to delaminations at the interfaces between the silicon, the adhesive, and the magnetics. Finite-element analysis modeling was performed to investigate the conditions of the rotor failure. Details of these simulations can be found in [21]. Although shape imperfections in the magnetic and the silicon structures might introduce stress concentrations, they were not included in the modeling, as it focused more on relative comparisons between different rotor configurations. Consequently, the results were used as guidelines for the rotor fabrication and assembly, rather than the absolute values of the maximum rotational speed before failure. The conditions of delaminations were also simulated [21]. It involved removing the bonded boundary condition on the contact faces of the PM pie piece with the silicon rotor frame and with the back iron. In this case, the epoxy and the interface between the back iron

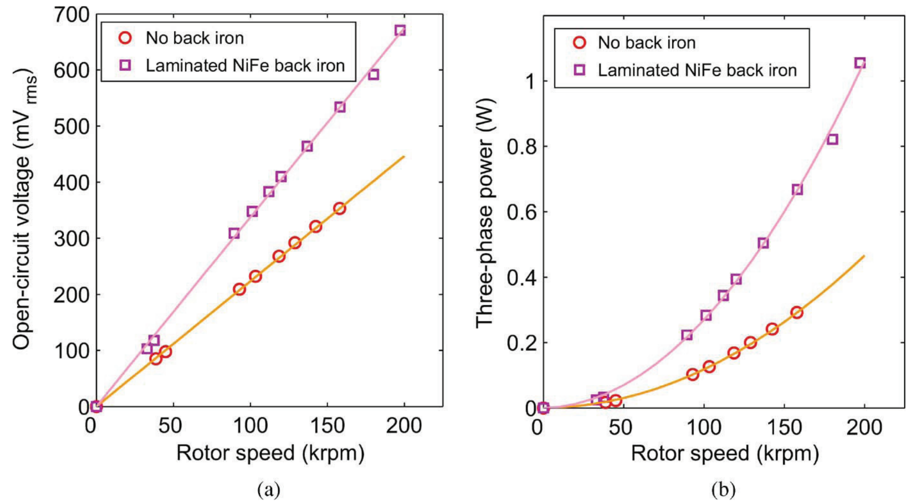

Fig. 15. (a) Open-circuit voltage and (b) power measurements as a function of rotor speeds up to 200 000 r/min using nonmagnetic and magnetic stators. The microgenerator with a laminated stator core generates 1.05 W at 200 000 r/min.

and the silicon fail at the same time. The bond between the silicon hub and the magnets is critical as the hub carries a significant amount of load through the bond. When this bond fails, the magnetic material will slide outward and load the silicon frame. The most critical parameter here is the maximum principal stress in the silicon frame (~400 MPa [21]) because the increased load will eventually stress the silicon up to a point where the outer rim will break off. The results indicated that the stress level in the silicon frame exceeded the yield strength at approximately 175 kr/min, which was in agreement with the experimental results. This was reflective of the fact that the silicon rim was unable to handle the full load of the magnetic components without assistance from the rotor hub.

C. Winding Resistance Measurements

The resistance and inductance of the microfabricated stator coils were measured using an impedance analyzer (Keithley 3322 LCZ Meter) in the frequency range of interest. The results are presented in Table I. The stator coil had a thickness of approximately 200 μm. The experimental rotational speed was limited to 200 000 r/min due to rotor failure. At such speeds, the inductance of the stator coil was negligible because the inductive reactance was small compared to the resistance. As a consequence, purely resistive loads can be used to assess maximum power generation.

D. Watt-Level Power Generation Using a Laminated Magnetic Stator

The microgenerators were electrically characterized as a function of the rotor speed. The devices with and without magnetic stator cores were tested. The two stator windings exhibited similar resistances of 320 mΩ and negligible inductances. The single-phase open-circuit voltage and the single-phase output power across a resistive load were measured simultaneously. The three-phase output power P_{3p} can be calculated as a function of the rms open-circuit voltage $V_{\rm oc}$, the winding resistance R_w, and the load resistance R_l, as introduced in the following equation [12]:

$$P_{3p} = 3 \times \frac{R_l \times V_{\rm oc}^2}{(R_w + R_l)^2}. \tag{2}$$

Equation (2) is maximized by selecting the load resistance such as $R_l = R_w$. Consequently, the calculated three-phase output power across a resistive load is

$$P_{3p} = \frac{3}{4} \times \frac{V_{\rm oc}^2}{R_w}. \tag{3}$$

In order to measure the output power, a load resistance of 0.32 Ω was connected across one single phase of the stator windings. The three-phase power is equal to three times the single-phase output power. The experimental testing was limited to rotational speeds of 200 000 r/min. The air gap was set at 100 μm by manual alignment. The fully integrated device supported by gas bearings delivered an open-circuit voltage per unit speed of 2.32 $\mathrm{mV_{rms}} \cdot (\mathrm{kr/min})^{-1}$ [20], which compares favorably with the voltage performance delivered by the silicon-package generator without a stator back iron, as shown in Fig. 15(a). Furthermore, the microgenerator with a laminated back iron demonstrated a 50% voltage increase, which corresponded to a power increase of 225%. The output power across a resistive load was measured, and the three-phase power is shown in Fig. 15(b). At 200 000 r/min, the device with laminated magnetic cores generated 1.05 W of output power across a resistive load. This corresponds to a power density of 9.5 $\mathrm{W \cdot cm^{-3}}$ ($OD = 10.24$ mm, $ID = 5.10$ mm, and $T = 1.4$ mm).

VII. Summary and Conclusion

In this paper, we have successfully demonstrated the silicon packaging of PM microgenerators, which offers compatibility with batch fabrication, as well as high-precision machining, a requirement for high rotational speeds and ultimate compactness of such power sources. The key elements were the following: 1) the fabrication of copper windings with through-wafer interconnects onto a nonplanar silicon structure; 2) the integration of vertically laminated electroplated magnetic cores for enhanced electrical performance; and 3) the conception of a heavy PM rotor with low imbalance for high rotational speeds. We have demonstrated that the 12-mm-diameter silicon rotor with inserted magnetics could sustain rotational speeds up to 200 000 r/min on an external spindle drive. The integration of a stator back iron increased the device output power by 225% for any rotational speed, and 1.05 W of output power was delivered across a resistive load at a maximum speed. In comparison, a rotational speed of 300 000 r/min would be required to generate the same output power using the microgenerator without magnetic laminations, corroborating the importance of an integrated stator back iron.

The successful packaging of PM microgenerators using silicon is a major step toward the development of a high-temperature microgenerator powered by hydrocarbon fuels, one of the potential solutions for a new generation of high-energy and high-power-density portable power sources.

References

[1] A. Epstein, S. D. Senturia, G. Anathasuresh, A. Ayon, K. Breuer, K.-S. Chen, F. Ehrich, G. Gauba, R. Ghodssi, C. Groshenry, S. Jacobson, J. Lang, C.-C. Mehra, J. Mur Miranda, S. Nagle, D. Orr, E. Piekos, M. Schmidt, G. Shirley, S. Spearing, C. Tan, Y.-S. Tzeng, and I. Waitz, "Power MEMS and microengines," in *Proc. 9th Transducers*, Jun. 1997, vol. 2, pp. 753–756.

[2] S. A. Jacobson and A. H. Epstein, "An informal survey of power MEMS," in *Proc. Int. Symp. Micro-Mech. Eng. 2003*, pp. 513–520.

[3] O. Cugat, J. Delamare, and G. Reyne, "Magnetic micro-actuators and systems (MAGMAS)," *IEEE Trans. Magn.*, vol. 39, no. 6, pp. 3607–3612, Nov. 2003.

[4] S. Das, D. P. Arnold, I. Zana, J.-W. Park, M. G. Allen, and J. H. Lang, "Microfabricated high-speed axial-flux multiwatt permanent-magnet generators—Part I: Modeling," *J. Microelectromech. Syst.*, vol. 15, no. 5, pp. 1330–1350, Oct. 2006.

[5] D. P. Arnold, S. Das, J.-W. Park, I. Zana, J. H. Lang, and M. G. Allen, "Microfabricated high-speed axial-flux multiwatt permanent-magnet generators—Part II: Design, fabrication, and testing," *J. Microelectromech. Syst.*, vol. 15, no. 5, pp. 1351–1363, Oct. 2006.

[6] H. Raisigel, O. Cugat, and J. Delamare, "Permanent magnet planar microgenerators," *Sens. Actuators A, Phys.*, vol. 130, pp. 438–444, Aug. 2006.

[7] D. P. Arnold, F. Herrault, I. Zana, P. Galle, J.-W. Park, S. Das, J. H. Lang, and M. G. Allen, "Design optimization of an 8 W, microscale, axial-flux, permanent magnet generator," *J. Micromech. Microeng.*, vol. 16, no. 9, pp. S290–S296, Sep. 2006.

[8] C. T. Pan and T. T. Wu, "Development of a rotary electromagnetic microgenerator," *J. Micromech. Microeng.*, vol. 17, no. 1, pp. 120–128, Jan. 2007.

[9] F. Herrault, C.-H. Ji, and M. G. Allen, "Ultraminiaturized, high-speed, permanent magnet generators for milliwatt-level power generation," *J. Microelectromech. Syst.*, vol. 17, no. 6, pp. 1376–1387, Dec. 2008.

[10] I. Zana, F. Herrault, D. P. Arnold, and M. G. Allen, "Magnetic patterning of permanent-magnet rotors for microscale motor/generators," in *Proc. 5th PowerMEMS*, Dec. 2005, pp. 116–119.

[11] D. P. Arnold, "Review of microscale magnetic power generation," *IEEE Trans. Magn.*, vol. 43, no. 11, pp. 3940–3951, Nov. 2007.

[12] F. Herrault, "Microfabricated air-turbine and heat-engine-driven permanent magnet generators," Ph.D. dissertation, Université de Toulouse—INSA, Toulouse, France, 2009.

[13] A. Holmes, G. Hong, and K. Pullen, "Axial-flux permanent magnet machines for micropower generation," *J. Microelectromech. Syst.*, vol. 14, no. 1, pp. 54–62, Feb. 2005.

[14] F. Herrault, C.-H. Ji, S.-H. Kim, X. Wu, and M. G. Allen, "A microfluidic-electric package for power MEMS generators," in *Proc. 21st IEEE MEMS*, Tucson, AZ, Jan. 2008, pp. 112–115.

[15] K. Isomura, S. Tanaka, S. Togo, and M. Esashi, "Development of high-speed micro-gas bearings for 3-D micro-turbo machines," *J. Micromech. Microeng.*, vol. 15, no. 9, pp. S222–S227, Sep. 2005.

[16] C. Lee, M. Liamini, and L. G. Frechette, "Design, fabrication, and characterization of a microturbopump for a Rankine cycle micro power generator," in *Proc. Solid-State Sensor, Actuator, Microsyst. Workshop*, Hilton Head, SC, Jun. 2006.

[17] A. H. Epstein, "Millimeter-scale, MEMS gas turbine engines," *ASME J. Eng. Gas Turbines Power*, vol. 126, pp. 205–226, Apr. 2004.

[18] C. J. Teo, L. X. Liu, H. Q. Li, L. C. Ho, S. A. Jacobson, F. F. Ehrich, A. H. Epstein, and Z. S. Spakovszky, "High-speed operation of a gas-bearing supported MEMS-air turbine," *J. Tribol.*, vol. 131, no. 3, pp. 032001-1–032001-9, Jul. 2009.

[19] F. Herrault, D. P. Arnold, I. Zana, P. Galle, and M. G. Allen, "High temperature operation of multi-watt, axial-flux, permanent-magnet generators," *Sens. Actuators A, Phys.*, vol. 148, no. 1, pp. 299–305, Nov. 2008.

[20] B. C. Yen, F. Herrault, K. J. Hillman, M. G. Allen, F. F. Ehrich, S. Jacobson, C.-H. Ji, J. H. Lang, H. Li, Z. S. Spakovsky, and D. R. Veazie, "Characterization of a fully-integrated permanent-magnet turbine generator," in *Proc. 8th PowerMEMS*, Dec. 2008, pp. 121–124.

[21] B. C. Yen, "A fully-integrated multi-watt permanent-magnet turbine generator," Ph.D. dissertation, EECS, MIT, Cambridge, MA, 2008.

[22] D. P. Arnold, F. Cros, I. Zana, D. R. Veazie, and M. G. Allen, "Electroplated metal microstructures embedded in fusion-bonded silicon: Conductors and magnetic materials," *J. Microelectromech. Syst.*, vol. 13, no. 5, pp. 791–798, Oct. 2004.

[23] N. P. Pham, J. N. Burghartz, and P. M. Sarro, "Spray coating of photoresist for pattern transfer on high topography surfaces," *J. Micromech. Microeng.*, vol. 15, no. 4, pp. 691–697, Apr. 2005.

[24] C.-H. Ji, F. Herrault, and M. G. Allen, "A metallic buried interconnect process for through-wafer interconnection," *J. Micromech. Microeng.*, vol. 18, no. 8, p. 085016, Aug. 2008.

[25] S. Linder, H. Baltes, F. Gnaedinger, and E. Doering, "Photolithography in anisotropically etched grooves," in *Proc. 9th IEEE MEMS*, Feb. 1996, pp. 38–43.

[26] F. Herrault, C.-H. Ji, S. Rajaraman, R. H. Shafer, and M. G. Allen, "Electrodeposited metal structures in high aspect ratio cavities using vapor deposited polymer molds and laser micromachining," in *Proc. 14th Transducers*, Jun. 2007, pp. 513–516.

[27] D. P. Arnold, I. Zana, and M. G. Allen, "Analysis and optimization of vertically oriented, through-wafer, laminated magnetic cores in silicon," *J. Micromech. Microeng.*, vol. 15, no. 5, pp. 971–977, May 2005.

[28] J.-W. Park and M. G. Allen, "Ultralow-profile micromachined power inductors with highly laminated Ni/Fe cores: Application to low-megahertz dc–dc converters," *IEEE Trans. Magn.*, vol. 39, no. 5, pp. 3184–3186, Sep. 2003.

[29] D. P. Arnold, "Magnetic machines for microengine power generation," Ph.D. dissertation, ECE, Georgia Inst. Technol., Atlanta, GA, 2004.

Florian Herrault received the B.S. and M.S. degrees in physics and materials science and the Ph.D. degree in electrical and electronics engineering from the National Institute of Applied Sciences (INSA), Toulouse, France, in 2003, 2005, and 2009, respectively. He worked on his Ph.D. research at Georgia Institute of Technology (Georgia Tech), Atlanta.

He is currently a Research Engineer with the MicroSensors and MicroActuators Group, Georgia Tech. His current research interests include piezoelectric and electromagnetic actuators, small-scale power generation systems, 3-D microelectromechanical systems (MEMS) fabrication, and MEMS-enabled thermal management.

Bernard C. Yen (S'05–M'08) received the B.S. degree in electrical engineering from the University of California, Berkeley, in 2003, and the Ph.D. degree in electrical engineering from the Massachusetts Institute of Technology, Cambridge, in 2008.

He is currently with BioScale, Inc., Cambridge, MA, developing MEMS-based biological sensors for viral, bacterial, and protein detection. His research interests include microelectromechanical systems (MEMS), energy harvesting, power electronics, and analog circuit design.

Chang-Hyeon Ji (M'07) received the B.S. and M.S. degrees in electrical engineering and the Ph.D. degree in electrical engineering and computer science from Seoul National University, Seoul, Korea, in 1995, 1997, and 2001, respectively. His doctoral dissertation concerned the design, fabrication, and testing of electromagnetic micromirrors for microphotonic applications.

From 2001 to 2006, he was with LG Electronics Institute of Technology, Seoul, where he developed microactuators for various types of applications, including optical communication and scanning laser display. He is currently a Postdoctoral Fellow at the Georgia Institute of Technology, Atlanta. His current research interests include micropower generation and energy scavenging, micromachined components and through-wafer interconnection technology for high-power electronics, nanofabrication technology, and biomicroelectromechanical systems.

Zoltan S. Spakovszky received the Dipl.Ing. degree in mechanical engineering from the Swiss Federal Institute of Technology (ETH) Zurich, Zurich, Switzerland, and the M.S. and Ph.D. degrees in aeronautics and astronautics from the Massachusetts Institute of Technology (MIT), Cambridge.

He is currently the H. N. Slater Associate Professor of Aeronautics and Astronautics at MIT and the Director of the Gas Turbine Laboratory. His principal fields of interest include internal flows in turbomachinery, compressor aerodynamics and stability, dynamic system modeling of aircraft gas turbine engines, microscale gas bearing dynamics, and aeroacoustics. He currently directs analytical and experimental research in these areas and teaches graduate and undergraduate courses in thermodynamics, propulsion and fluid mechanics, and aeroacoustics. He has authored a number of technical papers published in refereed journals.

Dr. Spakovszky is a Technical Consultant to industry and government agencies, acts as the Chair of the Turbomachinery Committee of the ASME International Gas Turbine Institute, and is an Associate Editor for the ASME *Journal of Turbomachinery*. He was the recipient of five ASME International Gas Turbine Institute Best Paper Awards, the ASME Melville Medal, a NASA Honor Award, and three AIAA Undergraduate Advising/Teaching Awards.

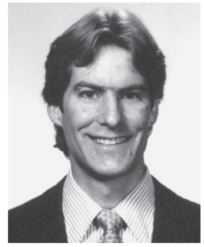

Jeffrey H. Lang (F'98) received the B.S., M.S., and Ph.D. degrees from the Department of Electrical Engineering and Computer Science, Massachusetts Institute of Technology (MIT), Cambridge, in 1975, 1977, and 1980, respectively.

In 1980, he joined the faculty of MIT, where he is currently a Professor of electrical engineering and computer science. Between 1991 and 2003, he served as the Associate Director of the MIT Laboratory for Electromagnetic and Electronic Systems. His research and teaching interests focus on the analysis, design, and control of electromechanical systems with emphasis on rotating machinery; microscale [microelectromechanical systems (MEMS)] sensors, actuators, and energy converters; flexible structures; and the dual use of electromechanical actuators as motion and force sensors. He has written over 220 papers and is the holder of 12 patents in the areas of electromechanics, MEMS, power electronics, and applied control. He is the coauthor of *Foundations of Analog and Digital Electronic Circuits* (Morgan Kaufman, 2005). He is the Editor of, and a Contributor to, *Multi-Wafer Rotating MEMS Machines: Turbines, Generators and Engines* (Springer, 2009).

Dr. Lang is a former Hertz Foundation Fellow. He served as an Associate Editor of *Sensors and Actuators* between 1991 and 1994. He was the recipient of four Best Paper Prizes from IEEE Societies. He was also the recipient of two teaching awards from MIT.

Mark G. Allen (M'89–SM'04) received the B.A. degree in chemistry, the B.S.E. degree in chemical engineering, and the B.S.E. degree in electrical engineering from the University of Pennsylvania, Philadelphia, and the M.S. and Ph.D. degrees from the Massachusetts Institute of Technology, Cambridge.

Since 1989, he has been with the School of Electrical and Computer Engineering, Georgia Institute of Technology (Georgia Tech), Atlanta, where he is currently a Regents' Professor and the J. M. Pettit Professor in Microelectronics, with joint appointment in the School of Chemical and Biomolecular Engineering. He is also the Senior Vice Provost for Research and Innovation and is in charge of overseeing Georgia Tech's interdisciplinary research centers, managing Georgia Tech's sponsored research portfolio, and guiding the commercialization of Georgia Tech research results and intellectual property. He is the Editor-in-Chief of the *Journal of Micromechanics and Microengineering*. His current research interests are in the fields of microfabrication and nanofabrication technology, with emphasis on new approaches to fabricate devices with characteristic lengths in the micro- to nanoscale from both silicon and nonsilicon materials. Examples include micromagnetics, high-temperature sensors, small-scale power generation, biofluidic microvasculatures and implantable microsensors, and the use of microstructures to create nanostructures.

Dr. Allen was the Cochair of the 1996 IEEE/ASME Microelectromechanical Systems Conference.